P. HVELPLUND

ENERGY LOSS AND STRAGGLING OF 100-500 keV ATOMS WITH $2 \leq Z_1 \leq 12$ IN VARIOUS GASES

Det Kongelige Danske Videnskabernes Selskab
Matematisk-fysiske Meddelelser **38, 4**

Kommissionær: Munksgaard
København 1971

Synopsis

The stopping cross section $S = \Delta E/N\Delta R$ and the reduced straggling $\Omega^2/N\Delta R$ for ions with $2 \leq Z_1 \leq 12$ in the 100–500 keV energy range was measured in helium, air, and neon. For $Z_1 = 2$ and $Z_1 = 8$, the stopping cross section was also measured in hydrogen and oxygen. The energy-loss distribution of the ions in the forward direction after penetration of a thin layer of gas contained in a differentially pumped gas cell was determined by means of a magnetic analyzer.

The previously found oscillatory dependence of the stopping cross section on the atomic number of the incident atom was also observed for the present target gases. Further, it was found that the stopping cross section for atoms with $Z_1 \leq 10$ is smaller in neon than in air. By including data of other investigators, the Z_2 dependence of the stopping cross sections for 100-keV He^4 and 200-keV O^{16} was investigated, and an oscillatory dependence with some similarity to the Z_1 oscillations was found.

At constant velocity, the energy straggling was found to be a monotonic function of Z_1. The straggling is compared with a theoretical prediction based on Firsov's equation for inelastic energy transfer in a single collision, and qualitative agreement is obtained.

PRINTED IN DENMARK
BIANCO LUNOS BOGTRYKKERI A/S

Introduction

The stopping cross section of heavy, charged particles of a few hundred keV has recently become a subject of renewed interest, see e.g. Ref. [1]. In spite of this, only a few investigations of energy-loss straggling have been reported[2,3], so it was decided to make a rather broad investigation of energy-loss distributions of heavy, charged particles at keV energies penetrating thin layers of gas.

The present paper, which is only a part of a larger experimental study, deals with the energy loss and energy straggling suffered by light ions ($2 \leq Z_1 \leq 12$) penetrating a layer of helium, air, and neon gas with energies from 100 to 500 keV, i.e. the energy region, where inelastic collisions are dominant in the slowing-down process. The remainder of the work will be published in two forthcoming papers, one of which will deal with energy-loss distributions in the velocity range, where the dominant mode of energy loss is elastic encounters between the projectile and the target atoms, and the other will deal with the energy-loss distribution of protons in the 100–500-keV energy range, where slowing-down is due to inelastic collisions and may be treated by quantum-mechanical perturbation methods.

The main reason for the renewed interest in stopping cross-section measurements in the region, where the electronic stopping cross section S_e is velocity-proportional, is the experimentally found oscillatory dependence of S_e versus the atomic number Z_1[4].

The nature of these oscillations have been subjected to various experimental tests both in random[3,5–9] and in crystalline materials [10–12]. So far, the most pronounced oscillations have been found in single crystals for the well-channeled part of the transmitted beam.

The fact that the ratio between maxima and minima in stopping cross sections in an oriented single crystal is much larger that that of an amorphous target indicates that the oscillations are influenced by the selection of impact parameters in the collisions contributing to the stopping power. In order to

gain further insight in the slowing-down process, especially in the Z_1 oscillations, it was decided to investigate the energy straggling as a function of Z_1. Straggling in a random material is more strongly influenced by the close collisions than is the stopping power. Therefore, straggling measurements are well suited for systematic investigations of the extent to which the close collisions contribute to e.g. the Z_1 oscillations in stopping power. In the present paper, straggling is reported for projectiles with $2 \leq Z_1 \leq 12$ in helium, air, and neon.

Stopping power can, of course, be obtained simultaneously from the experimetal data, and therefore also atomic stopping cross sections for the same combinations of projectile and target gas are reported.

As the present measurements include stopping cross sections in neon, where no previous measurements exist for projectiles heavier than protons, and also because of the growing interest in the Z_2 dependence of the stopping cross sections[1,13], it was decided to investigate this dependence in further detail. Therefore, stopping cross-section measurements of He^4 and O^{16} have been extended to other gases (hydrogen, helium, air, oxygen, and neon). A discussion of the Z_2 dependence of the stopping cross sections is given on the basis of the existing data for 100-keV He^4 and 200-keV O^{16}, together with the values reported in this paper.

II. Theory

The penetration of charged particles through matter is normally treated by dividing the collisions into electronic and nuclear collisions (Ref. 14). The scattering of a particle is always dominated by nuclear collisions, whereas its energy loss in the present velocity range is mostly due to electronic collisions. Energy straggling is a more complicated problem to treat theoretically because the electronic and nuclear collisions cannot be considered to be independent. The energy straggling measured in the present experiment is, however, (as shown in section IV E), mainly determined by electronic collisions.

A. Energy Loss.

A theoretical treatment of electronic stopping at low velocities has been given by Lindhard and Scharff[15]. On the basis of the Thomas-Fermi statistical model, they calculated the electronic stopping cross section valid for ion velocities lower than $v_0 Z_1^{2/3}$

$$\left.\begin{aligned} S_e &= \xi_e 8\pi e^2 a_0 (Z_1 Z_2 / Z) \frac{v}{v_0} \\ (Z^{2/3} &= Z_1^{2/3} + Z_2^{2/3}), \end{aligned}\right\} \quad (1)$$

where a_0 and v_0 are the Bohr radius and the Bohr velocity, respectively, Z_1 and Z_2 the atomic numbers of projectile and target, e the electron charge, and ξ_e a constant of the order of 1–2, which may vary approximately as $Z_1^{1/6}$.

At veloties around v_0, LINDHARD et al.[16] have shown that the nuclear collisions also contribute to the slowing-down of atoms, and the total stopping cross sections may then be written

$$S = S_e + S_n, \quad (2)$$

where S_n is the stopping cross section for nuclear collisions.

From a semiclassical Thomas-Fermi treatment, FIRSOV[17] calculated the inelastic energy transfer as a function of impact parameter:

$$T(p) = \frac{(Z_1 + Z_2)^{5/3}\, 4.3\, 10^{-8} v}{[1 + 3.1 (Z_1 + Z_2)^{1/3} 10^7 p]^5}\, [eV] \quad (3)$$

valid when the atomic numbers of the colliding particles differ by no more than a factor of 4. p is the impact parameter in cm and v the velocity in cm/sec. From this formula, the electronic stopping cross section can be calculated as shown by TEPLOVA et al.[18]:

$$S_e = \int_0^\infty T(p) 2\pi p\, dp = 5.15 (Z_1 + Z_2) 10^{-15} \left(\frac{v}{v_0}\right) eV\,\mathrm{cm}^2/\mathrm{atom} \quad (4)$$

B. Energy Straggling

When an initially monoenergetic beam passes through matter, the statistical nature of collision processes will cause an energy spread in the beam. The mean square deviation Ω^2 of the energy distribution, commonly called the energy straggling, is, as shown by BOHR[14], given by

$$\Omega^2 = N \Delta R \int T^2 d\sigma, \quad (5)$$

where $N \Delta R$ is the number of atoms per cm^2, T the energy transfer in a single collision, and $d\sigma$ the cross section for the energy transfer T. Here it is assumed that the energy is changed only little when passing the stopping layer. Under the further assumption that the energy transfer is a function of the impact parameter only, the straggling can be calculated as

$$\Omega^2 = N\Delta R \int_0^\infty T^2(p)\, 2\pi p\, dp\,. \tag{6}$$

When FIRSOV's value for the inelastic energy transfer (Eq. (3)) is inserted, the electronic straggling is

$$\Omega^2 = N\Delta R\, 8(Z_1 + Z_2)^{8/3} 10^{-15} \left(\frac{v}{v_0}\right)^2 eV^2\,\mathrm{cm}^2/\mathrm{atom}\,. \tag{7}$$

III. Experimental

The ion beams used in this experiment were produced by the Aarhus 600-keV heavy-ion accelerator. After acceleration and deflection in a 75° double-focusing sector magnet, the beam entered the differentially pumped target region through small apertures. Having passed the target area, the beam was energy-analyzed by means of an analyzing magnet and detected by an open electron multiplier (see Fig. 1).

A. Stopping Cell and Gas Equipment

The stopping cell consists of a differentially pumped gas cell, 828 mm ± 1 mm long and 100 mm in diameter. The gas cell has 1-mm apertures (A) in both ends, and 2-mm apertures (B) separating the differentially pumped region from the high vacuum (Fig. 1). Aperture C in Fig. 1 defines the beam divergence to within one third of a degree.

Helium, air, and neon were used as target gases. Dried atmospheric air was let in through a needle valve, while helium and neon were taken from steel flasks, where the pressure was held a little above 1 atm. These flasks were connected to the gas cell through a servo-controlled magnet valve. The control signal to the valve was supplied by an oil manometer[19], measuring the pressure in the gas cell. By this arrangement, the pressure could be kept constant to within 0.1 percent for sufficient time for the recording of the energy distribution. By the commercial supplier, the purities of the gases used were stated to be as follows: helium 99.9992 % and neon 99.99 %.

The target pressure, normally around 0.1 torr, was measured with a McLeod manometer (Consolidated Vacuum Corporation, type GM-100A) with a systematic error smaller than 2 %. The outside pressure (regions AB, Fig. 1) was found to be 0.1 % of the target pressure, and since the total distance AB + BA is only one third of the distance BB, no correction for this effect was made. The target temperature was measured with a thermometer in close contact with the gas cell.

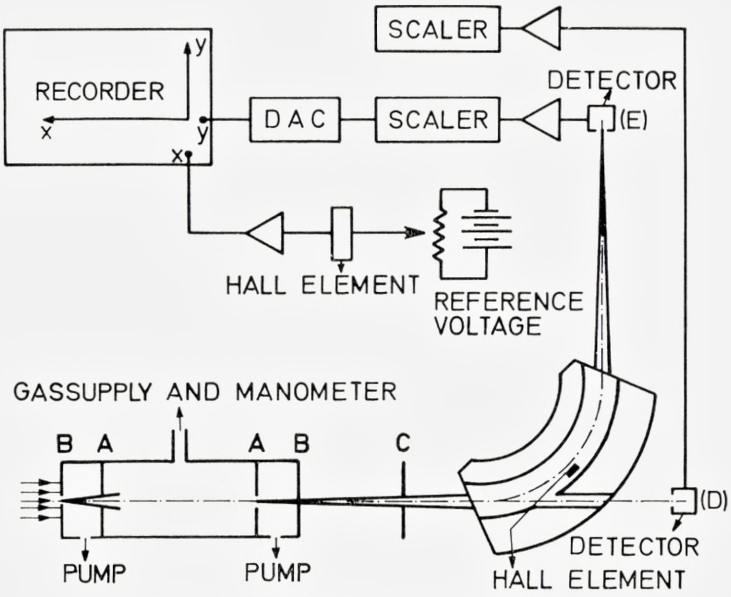

Figure 1. General diagram of the apparatus.

B. Analyzing Magnet, Detectors, and Electronic Equipment

The analyzing magnet is a double-focusing sector magnet. The magnetic field was measured with a Hall probe, which, in turn, was calibrated against a resonance probe. The field measured with the Hall probe (to within $\pm 0.4\,\%$) was fed to the x axis of an xy recorder. The deflected ions were detected with an open multiplier E (Fig. 1), and the undeflected neutral atoms were counted with a second open multiplier D (Fig. 1) for beam normalization during the period of measurement. The sensitive length of detector E was ~ 1 mm, perpendicular to the magnetic field, giving an energy resolution of $\sim 0.1\,\%$. The electronic equipment is shown in Fig. 1. The intensity of the deflected beam was plotted as a function of magnetic field by means of an yx curve plotter.

C. Determination of Energy Loss and Straggling

At each energy, a momentum spectrum was obtained with and without gas in the target chamber, cf. Fig. 2. The energy loss ΔE_0 was calculated under the assumption that the energy E of the transmitted beam is related to the magnetic field B by the equation $E = kB^2$, where k is a constant. On the basis of this equation, the most probable energy loss can be calculated as follows:

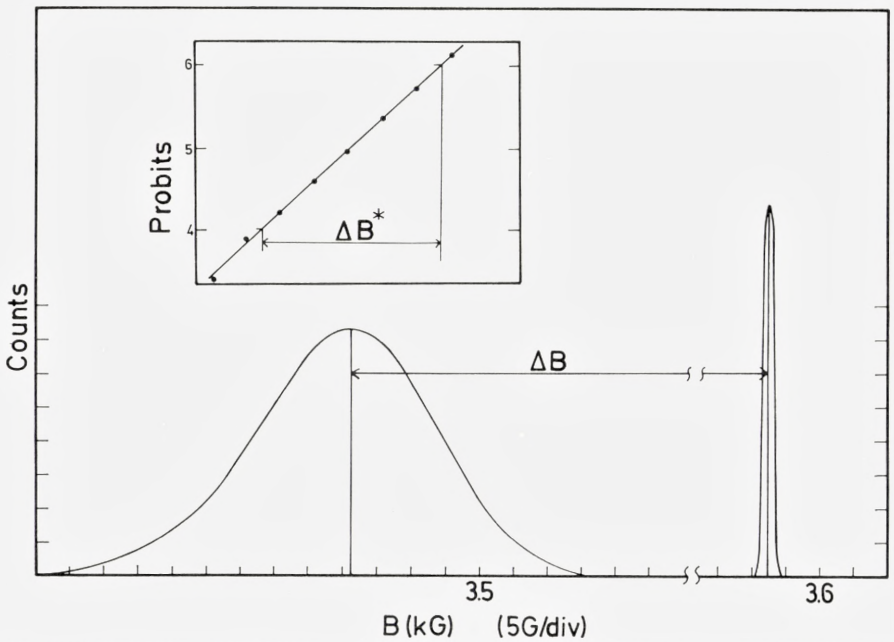

Figure 2. Momentum distributions of an incident 200 keV carbon beam and the same beam emerging from a 3.9 10^{17} atoms/cm^2 neon layer. ΔB is the reduction in the magnetic field corresponding to the two peak values. The latter distribution is transformed into a straight line on probability paper, and twice the standard deviation ΔB^* can be read directly.

$$\Delta E_0 = E_i \frac{\Delta B}{B_i}\left(2 - \frac{\Delta B}{B_i}\right), \tag{8}$$

where B_i is the analyzer magnetic field corresponding to the peak in the momentum distribution without gas in the target chamber, and $\Delta B/B_i$ the corresponding relative reduction in magnetic field for the peak of the momentum distribution with gas in the target chamber. E_i is the energy of the incident beam.

For small values of $\Delta B/B$, the approximate relation

$$\Delta E = 2E \frac{\Delta B}{B}, \tag{9}$$

where E and B are corresponding values, can be used. This means that over a short distance, the B axis can be considered an energy axis. This approximation is used in the calculation of the standard deviations of the distributions, where normally $\Delta B/B < 0.01$. The energy-distribution curve is expected to

be Gaussian in shape, and therefore the integral distribution was plotted on probability paper (Fig. 2). From the straight line, the standard deviation Ω_2 was easily obtained as

$$\Omega_2 = E\frac{\Delta B^*}{B}. \tag{10}$$

The standard deviation of the primary energy distribution Ω_1 is experimentally found to be

$$\Omega_1 = \frac{E}{2300}. \tag{11}$$

The straggling is given by

$$\Omega^2 = \Omega_2^2 - \Omega_1^2, \tag{12}$$

since the standard deviations add up geometrically.

In all cases reported here, Ω_1 is small compared to Ω_2, i.e. the exact magnitude of Ω_1 is not important.

The number of molecules per cm^2 is

$$N\Delta R = A\,L\frac{273}{(T+273)}\frac{P}{760}. \tag{13}$$

where $A = 2.687\ 10^{19}$ molecules/atm cm^3 is Loschmidt's constant, L the length of the gas cell, T the temperature in °C, and P the pressure in mmHg.

The observed stopping cross section S_0 is defined as

$$S_0 = \frac{\Delta E_0}{N\Delta R}, \tag{14}$$

at the energy $E = E_i - \Delta E_0/2$, and the reduced straggling is defined as $\Omega^2/N\Delta R$ at the same energy.

The non-systematic errors are as follows:

(i) uncertainties in the determination of ΔE and Ω (mainly uncertainties in ΔB): 3 %,
(ii) uncertainty in gas pressure: 3 %, and,
(iii) uncertainty in the temperature measurements: 1 %.

The uncertainty of E_i is $\sim$ 0.1 %.

IV. Results and Discussion

A. Values of Stopping Cross Sections

The measured stopping cross section S_0 is corrected for nuclear stopping in the way shown by FASTRUP et al.[7] . Here, the measured stopping cross section is assumed to be the sum of the electronic stopping cross section S_e and the partial nuclear stopping cross section S_n^*, corresponding to the most probable energy loss in nuclear collisions, i.e.

$$S_0 = S_e + S_n^* . \tag{15}$$

For details, see ref. 7). In the measurements reported here, the corrections for nuclear collisions are smaller than 10 % and in most cases can be neglected.

Figure 3 shows the electronic stopping cross section of Li^7 in neon as a function of energy. It is observed that the experimental values over the energy interval investigated are well described by a straight line on a log-log plot. This is valid for all the target-projectile combinations investigated, except for He^4 in hydrogen.

The results for the electron stopping cross sections are listed in Table I in the convenient form of

$$S_e = kE^P , \tag{16}$$

where k and P are constants.

It is estimated that the correct stopping cross section lies within $\pm$ 5 % of the best straight line through the experimental points.

B. Comparison with Other Experiments

WEYL[20] has measured the stopping cross sections for He^4, N^{14}, and Ne^{20} projectiles in helium and air in the 150- to 400-keV energy interval. In the cases where helium is used as target gas, the agreement with the present results is better than 2 %. On the other hand, WEYL's results lie approximately 10 % higher than the present values for He^4 and N^{14} in air, and 20 % higher for Ne in air. The fact that WEYL did not correct for nuclear stopping partly explains this discrepancy. ALLISON and LITTLEJOHN[21] have measured the stopping cross section for Li ions in helium and air in the 100- to 500-keV energy interval. In helium, the agreement is within 2 %, but their results in air lie 10 % below the present results.

For $6 \leq Z_1 \leq 12$ and with air as target gas, the present data may be compared with the data reported by FASTRUP et al.[9]), where the same experimental setup was used. The older data lie from 10 % to 16 % above the present results.

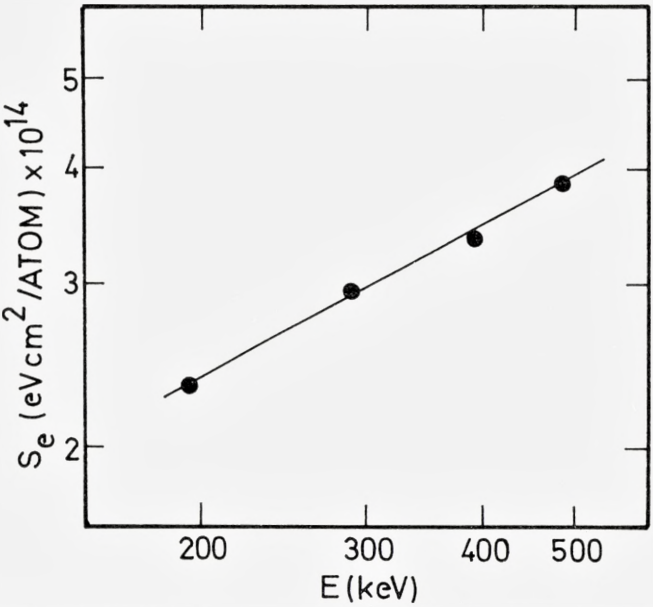

Figure 3. Electronic stopping cross section S_e versus energy for Li^7 in neon.

This discrepancy is difficult to understand, but it should be mentioned that in the present experiment, a McLeod gauge was connected to the experimental setup so that the actual pressure could be read directly. In the older experiment, the pressure was measured with a membrane manometer, which afterwards was calibrated against a McLeod gauge, and most likely a change in the membrane manometer may have taken place between the time of the measurements and the calibration.

Since the stopping power is the same (within experimental error) in air and oxygen, it should be possible also to compare the present stopping cross sections in air with ORMROD's values[6] for stopping cross sections in nitrogen. At ~ 200 keV, his data lie from 0 % to 6 % above the data obtained in this experiment.

With neon as target gas, no other experimental data are available for comparison.

The conclusion is that all available stopping-power data with helium as target gas agree to within 2 %, whereas the experimental data with air as target gas scatter much more than the quoted experimental errors.

TABLE I.

Experimental values of exponent P and coefficient k in $S_e = kE^P$, S_e in (eV cm²/atom) and E in (keV).

Projectile \ Gas	Air		He		Ne		Energy Interval (keV)
	$k \cdot 10^{15}$	P	$k \cdot 10^{15}$	P	$k \cdot 10^{15}$	P	
He^4	5.14	0.33	0.802	0.51	3.48	0.38	100 – 500
Li^7	1.15	0.60	0.136	0.77	1.29	0.55	100 – 500
Be^9	1.95	0.53	...	...	3.00	0.43	200 – 500
B^{11}	2.12	0.55	0.50	0.59	1.74	0.55	200 – 500
C^{12}	3.93	0.46	1.30	0.50	1.88	0.56	200 – 500
N^{14}	4.13	0.47	1.20	0.51	2.35	0.53	200 – 500
O^{16}	3.97	0.46	1.77	0.44	3.29	0.48	200 – 500
F^{19}	2.75	0.49	1.48	0.43	4.00	0.43	200 – 500
Ne^{20}	1.96	0.53	0.74	0.53	1.79	0.56	200 – 500
Na^{23}	1.08	0.61	0.286	0.63	1.86	0.53	200 – 500
Mg^{24}	0.663	0.67	0.133	0.70	0.93	0.63	200 – 500

Projectile \ Gas	O_2		H_2		Energy Interval (keV)
	$k \cdot 10^{15}$	P	$k \cdot 10^{15}$	P	
He^4	5.08	0.34			100 – 300
O^{16}	3.35	0.49	0.446	0.61	100 – 300

He^4 in H_2

E (keV)	$S_e \times 10^{14}$ eV cm²/atom
100	0.62
150	0.80
200	0.93
300	1.08

C. Z_1 Dependence of Stopping Cross Section

Figures 4 and 5 show S_e versus Z_1 in different target gases at a constant velocity $0.9\, v_0$ of the projectile, together with the theoretical curves by LINDHARD and SCHARFF[15] . It is observed that in all cases, the experimental curves are below theoretical estimates, as was found earlier by ORMROD[6] and FASTRUP et al.[9] in gaseous targets. Further, it is seen that the experimental curves

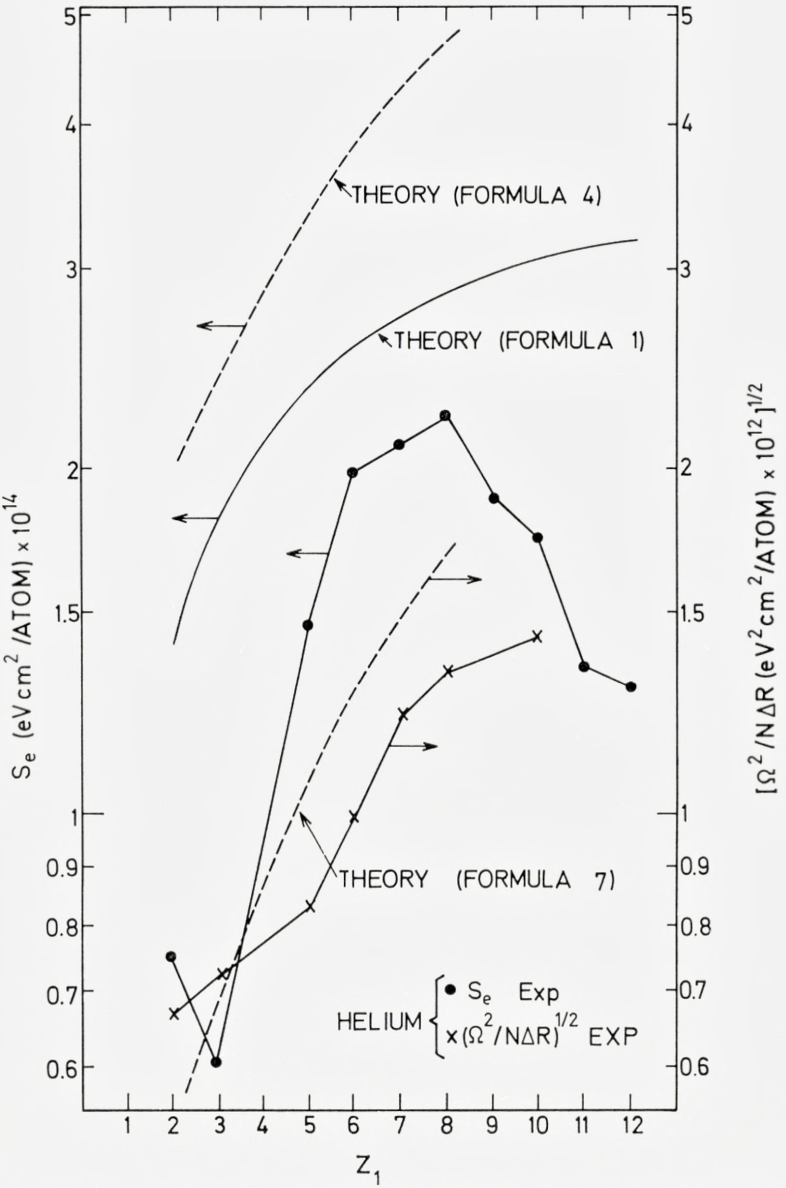

Figure 4. Electronic stopping cross section and straggling values at constant velocity (0.9 v_0) for a helium target, as a function of Z_1.

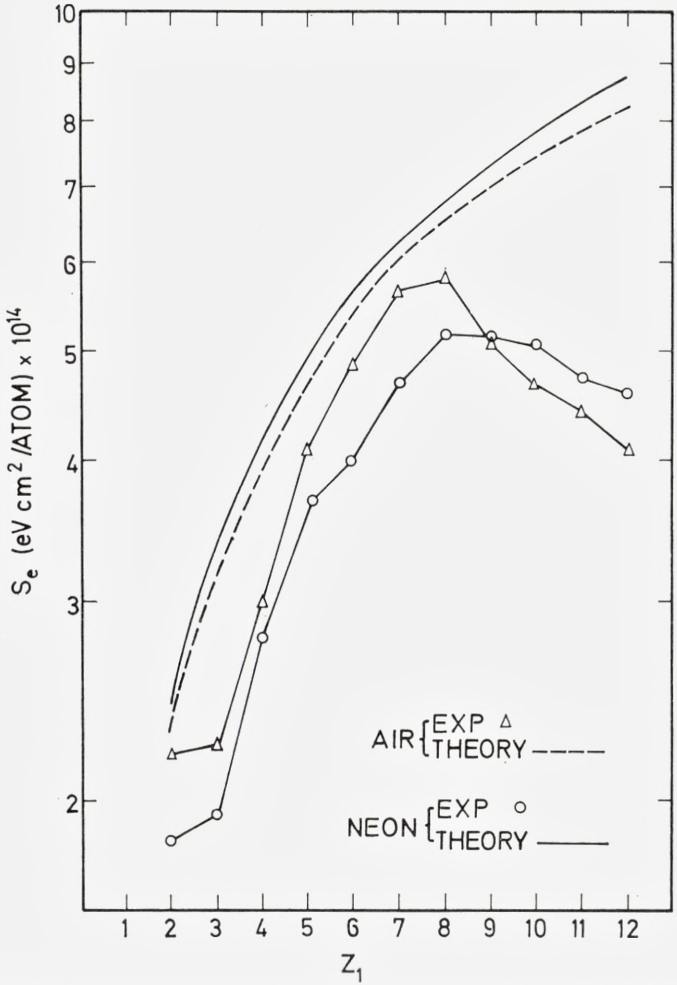

Figure 5. Electronic stopping cross section values at constant velocity (0.9 v_0) for an air target and a neon target, as a function of Z_1. Theoretical curve from equation (1).

exhibit oscillations similar to those found in single crystals and in other solid and gaseous targets. The positions of maxima and minima are roughly the same as those found by others in various target materials.

D. Z_2 Dependence of Stopping Cross Section

Figure 5 shows that for a given projectile and energy, the stopping power is smaller in neon than in atmospheric air for $Z \leq 9$. Also in cases where

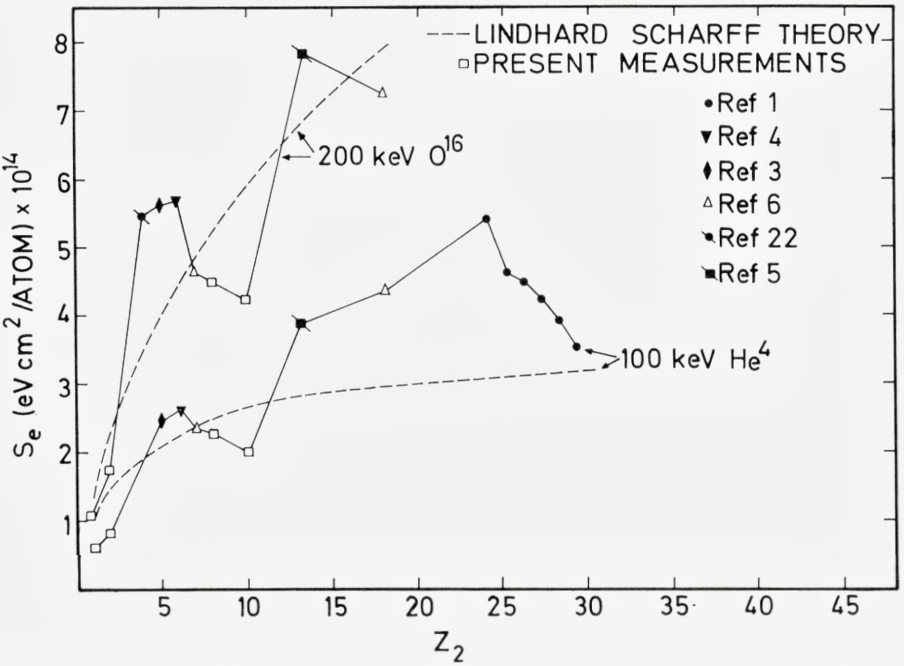

Figure 6. Electronic stopping cross section versus Z_2. The experimental values are partly from this paper and partly measured or interpolated values from Refs. 1, 3, 4–6 and 22. Theoretical curves from equation (1).

there is an energy overlap with ORMROD's[6] measurements of stopping power in nitrogen, the same decrease in stopping power is observed when going from nitrogen to neon.

Based on the stopping cross sections measured by others[1,3,4-6,22] and on present results, Fig. 6 shows the variation in stopping cross section for 200-keV O^{16} ions and 100-keV He^4 ions. The velocity of the ions is well below $v_0 Z_1^{2/3}$, and the stopping cross sections may be compared with the theoretical values given by Eq. (1). It should be mentioned here that the relative uncertainty in a plot of S_e versus Z_2 is larger compared with a plot of S_e versus Z_1, due to the difficulty of measuring the absolute thickness of the targets. In spite of this, at a given energy S_e clearly demonstrates an "oscillatory" dependence on Z_2. It is observed that the theoretical curves represent good mean values of the experimental points and that the Z_2 "oscillations" have some similarity to the Z_1 oscillations.

Recently, various groups have investigated the stopping power for a given projectile as a function of target material. WHITE and MUELLER[1] measured

the stopping power of H^1 and He^4 in Cr, Mn, Fe, Ca, Ni, and Cu at 100 keV and found, by collecting all stopping-power data for 100-keV protons, that the stopping power exhibits an oscillatory dependence on Z_2 with minima at $Z_2 = 10$ and $Z_2 \simeq 30$.

BERNHARD et al.[13] have measured stopping cross sections for Li ions in C, Al, Ti, and Cu, and in comparison with the data of others, they obtain a characteristic Z_2 dependence for the stopping power. They conclude that the dependence of the electronic stopping cross section on the atomic number of the target atom may be influenced by the structure of the target, i.e. by the target being in the gas phase or in the solid phase. This statement is not strongly supported by Fig. 6, but this is possibly due to the higher velocities compared with the velocity used by BERNHARD et al.[13], ($v \sim 0.4\, v_0$). The abrupt change in S_e from carbon to nitrogen, which BERNHARD et al. took as a support of the dependence of S_e on the target density, decreases when the energy is increased (see Refs.[4] and [6]).

E. Energy Straggling

Like the stopping cross section, the measured energy straggling also depends on both the elastic and the inelastic energy transfer to the target atoms, but in a more complex way. In the present velocity range, range straggling is normally attributed to nuclear collisions only[23]. In the present experiment, however, particles which have experienced violent nuclear collisions with target atoms, are scattered out of the small acceptance angle of the analyzing magnet and do not contribute to the observed energy-loss distribution.

In order to illustrate what is measured in this experiment, an example will be calculated. Figure 7 shows the energy transfer in a collision as a function of the impact parameter. The inelastic energy loss is calculated from Eq. (3), and the elastic energy transfer is calculated from a power potential $V(r) \propto r^{-2}$ (see Ref. 16). Also shown is the total energy transfer.

The angular distribution of the particles emerging from the target gas may be divided into a Gaussian peak and a tail. Collisions involving individual deflection angles smaller than φ^* produce the Gaussian distribution, and collisions with deflection angles larger than φ^* produce the tail distribution.

A good first-order estimate of φ^* is, as shown by Bohr[14], the standard deviation of the Gaussian distribution, i. e.

$$(\varphi^*)^2 \approx N\Delta R \int_0^{\varphi^*} \varphi^2 d\sigma, \tag{17}$$

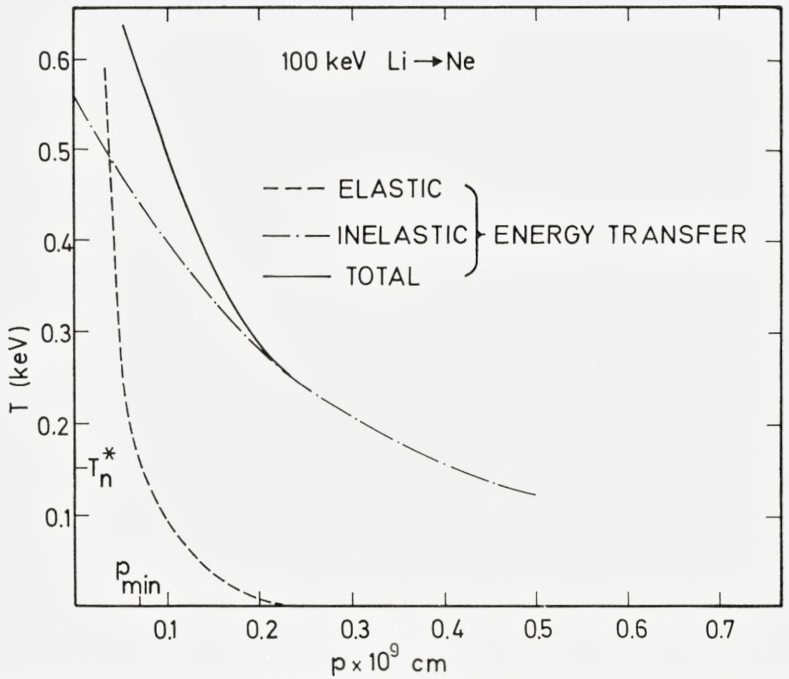

Figure 7. Energy transfer in a single collision as a function of the impact parameter. Inelastic energy transfer from equation (3). The elastic energy transfer is calculated from a power potential $V(r) \propto r^{-2}$ [16]. T_n^* and $p_{\min}$ refer to the maximum elastic energy transfer, and the corresponding impact parameter for atoms still belonging to the forward-directed beam as defined in text. ($N\Delta R = 5 \cdot 10^{17}$ atoms/cm^2).

where $d\sigma$ is the differential scattering cross section for an angular deflection φ. For $\varphi^* \ll 1$, which is normally the case,

$$(\varphi^*)^2 \sim \frac{M_2 T_n^*}{M_1 E}, \tag{18}$$

where T_n^* is the nuclear energy transfer from the projectile with mass M_1 to the target atom with mass M_2.

Now, since the acceptance angle is small compared to φ^* (i.e. $\sim 0.1\varphi^*$), the particles accepted by the analyzer will be those experiencing collisions in the energy interval $0 < T < T_n^*$.

In Fig. 7, T_n^* is shown for the actual case. If the straggling is now calculated as

$$\Omega^2 = N\Delta R \int_{p_{\min}}^{\infty} 2\pi p (T_n + T_e)^2 dp, \tag{19}$$

where $p_{\min}$ is defined as the impact parameter corresponding to the nuclear energy transfer T_n^*, then in the actual case, 100 keV Li in Ne ($N\Delta R = 5 \times 10^{17}$ atoms/cm^2),

$$\Omega > T_n^* + T_e(p_{\min}). \tag{20}$$

This means that one would expect a Gaussian energy distribution for the forward-directed beam. If the foundation of these calculations is accepted, the elastic part of the collisions will contribute with less than 10 % to the measured straggling Ω^2. On the other hand, the straggling resulting from inelastic collisions with impact parameters smaller than $p_{\min}$ is excluded. In the present example, this also amounts to $\sim$ 10 %, so the straggling in the forward-directed beam is, as described above, a rather well-defined quantity, mainly determined by inelastic collisions.

As the elastic and inelastic part of a collision cannot be treated as two independent collisions, it is difficult to separate the straggling into an electronic and a nuclear part as is done for the stopping cross section. Therefore no corrections for nuclear straggling have been applied for the straggling measurements.

Figure 8 shows the experimental values of $\Omega^2/N\Delta R$ for different projectiles in helium and air together with the theoretical curve as calculated from Eq. 7. It should be mentioned that the energy distribution curves for low energy and large Z_1 are slightly asymmetric. This is attributed to the fact that $\Omega < T_n^* + T_e(p_{\min})$ which, according to Bohr[14], should give rise to an asymmetric energy distribution. Each of the experimental points is an average of at least two experimental measurements. The values of $\Omega^2/N\Delta R$, read from a smooth curve through the experimental points, are given in Table II.

It is estimated that apart from probable mixing from nuclear collisions, the correct straggling values lie within $\pm$ 10 % of the values given by the smooth curves through the data of Fig. 8.

Due to the linear dependence of $\dfrac{\Omega^2}{N\Delta R}$ on E in a log-log plot found in most cases (Fig. 8), it seems justified to assume the following equation for the energy dependence of the straggling for a fixed target-projectile combination:

$$\frac{\Omega^2}{N\Delta R} = k_1 E^{P_1}. \tag{21}$$

Equation (7) indicates that the theoretical value of P_1 is unity. Table III shows the experimental P_1 values for the four low-Z projectiles, since here

TABLE II. Relative straggling $\Omega^2/N\Delta R$ in units of 10^{-12} eV^2 cm^2/atom.

Projectile	Energy (keV)	Gas He	Gas Air	Gas Ne
	100	0.54	2.4	1.85
	200	0.94	4.4	3.6
He^4	300	1.40	5.6	4.9
	400	1.80	6.4	5.7
	500	..	6.9	6.4
	100	0.38	2.1	..
	200	0.77	4.4	..
Li^7	300	1.13	6.9	..
	400	1.55	9.2	..
	500	1.93	11.0	..
	200	0.65	5.8	3.6
B^{11}	300	0.94	8.0	5.2
	400	1.42	9.7	6.9
	500	1.80	..	..
	200	0.86	7.6	4.7
C^{12}	300	1.16	12.0	7.4
	400	1.45	16.0	9.6
	500	1.70	20.0	11.8
	200	1.20	9.8	6.0
N^{14}	300	1.63	12.6	8.8
	400	2.05	16.0	11.0
	500	2.40	19.5	13.9
	200	1.25	10.6	8.1
O^{16}	300	1.75	13.6	10.2
	400	2.20	17.8	13.0
	500	2.80	22.4	16.8
	200	1.28	11.5	12.2
Ne^{20}	300	1.65	14.0	13.8
	400	2.10	18.3	16.1
	500	2.65	22.0	19.2
	200	..	10.0	12.0
Mg^{24}	300	..	13.0	12.9
	400	..	15.5	16.2
	500	..	18.8	19.5

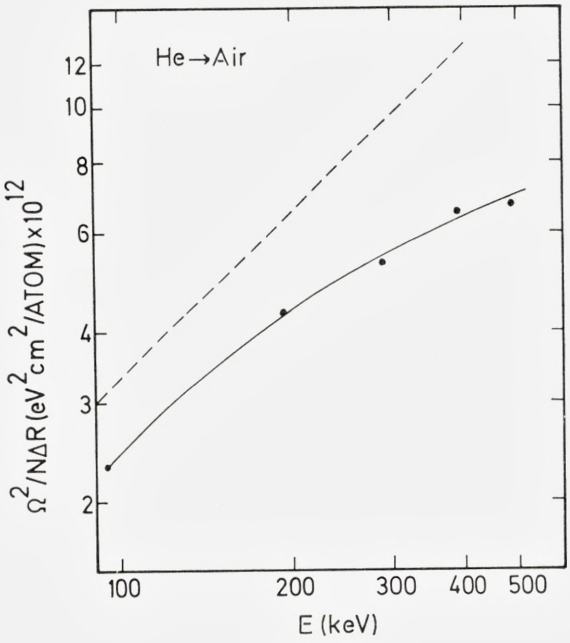
He→Air
12
10
8
6
4
3
2
100
200
300
400
500
E (keV)
$\Omega^2/N\Delta R\,(eV^2cm^2/ATOM)\times10^{12}$

8 a.

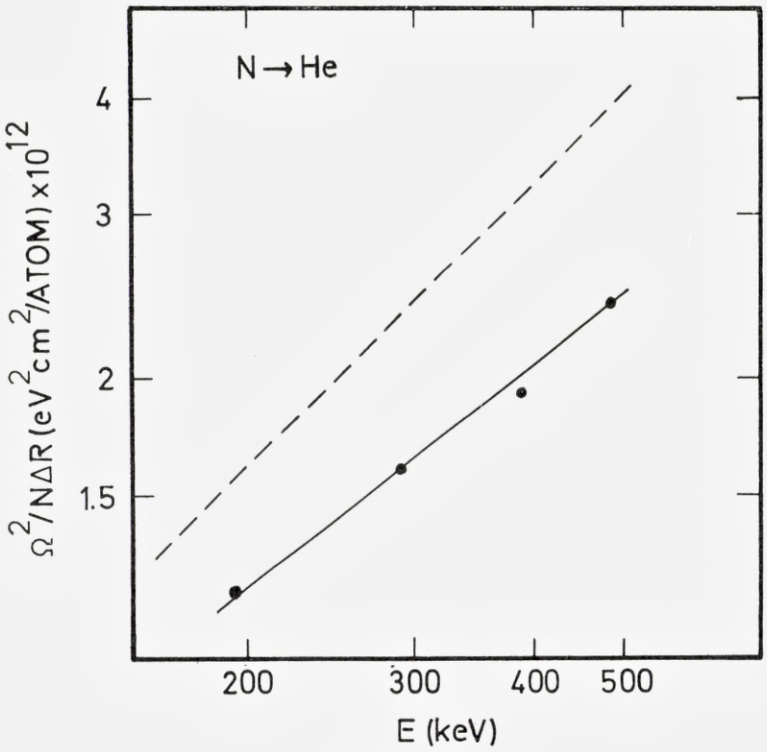
N→He
4
3
2
1.5
200
300
400
500
E (keV)
$\Omega^2/N\Delta R\,(eV^2cm^2/ATOM)\times10^{12}$

Fig. 8 c.

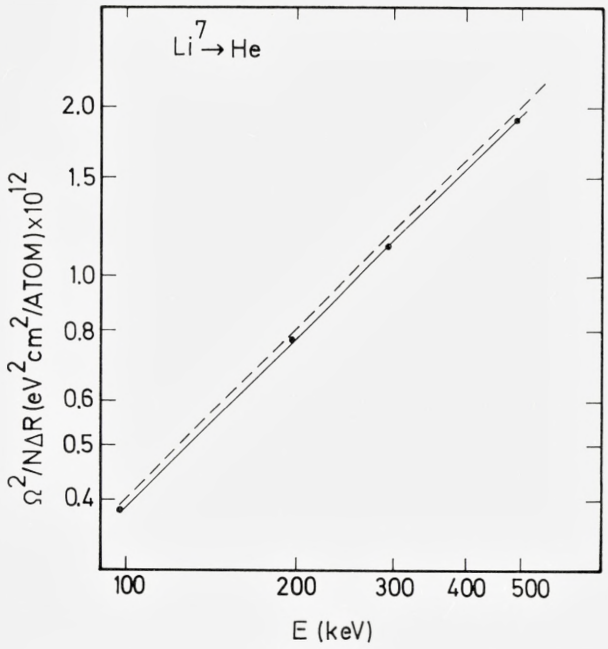

Fig. 8 b.

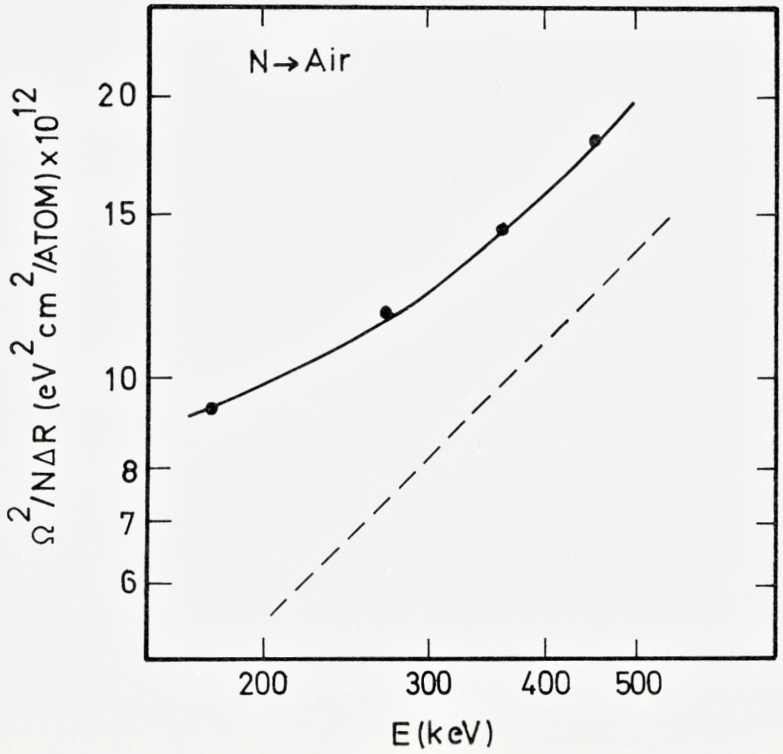

Fig. 8 d.

Figure 8. Relative straggling $\Omega_2/N\Delta R$ versus energy. Theoretical curves from equation (7).

TABLE III. Experimental values of exponent P_1 in $\Omega^2/N\Delta R = k_1 E^{P_1}$.

Projectile \ Gas	He	Air	Ne
He^4	~ 0.87	0.86	0.95
Li^7	1.00	1.02	–
B^{11}	1.25	0.74	0.92
C^{12}	0.74	1.04	0.95

the contribution from nuclear collisions is expected to be negligible. It is seen that the experimental values are fairly close to the theoretical value $P_1 = 1$. With He^4 as projectile, only the experimental values at 100 and 200 keV are used for the determination of P_1 because the points at higher energies fall outside the region of the validity of Eq. (7). The upward bend of the experimental curves at low energies for $Z_1 > 6$ is believed to be caused by an increasing mixture from nuclear collisions with decreasing energy.

On Figure 4, $(\Omega^2/N\Delta R)^{1/2}$ is plotted together with the stopping cross section S_e at a constant velocity $v = 0.9\, v_0$ as a function of Z_1. It is noticed that the straggling (contrary to the stopping power) is a monotonic function of Z_1. Further it is observed that the Z_1 oscillations in straggling, if any, are much less pronounced compared with the Z_1 oscillations found for S_e. This may indicate that a statistical model of the atom is well suited for describing straggling, with its enhanced dependence on collisions with small impact parameters compared with the stopping power.

Figure 9 shows the straggling $\Omega^2/N\Delta R$ at a constant velocity $v = 0.9\, v_0$ plotted for different target-projectile combination as a function of $(Z_1 + Z_2)$. It is observed that the straggling for a fixed energy and projectile is smaller in neon than in air. The deviation is larger for $Z_1 \sim 7$, just as was the case for the stopping cross section. Although large deviations exist between theory and experiment, Fig. 9 shows that the theoretical curve represents a good mean curve to the present experimental points.

V. Conclusions

Stopping power measurements in single crystals and in amorphous targets, together with this investigation of energy straggling, demonstrate that the Z_1 oscillations depend strongly on the relative importance of collisions with various impact parameters. The most pronounced oscillations have been found

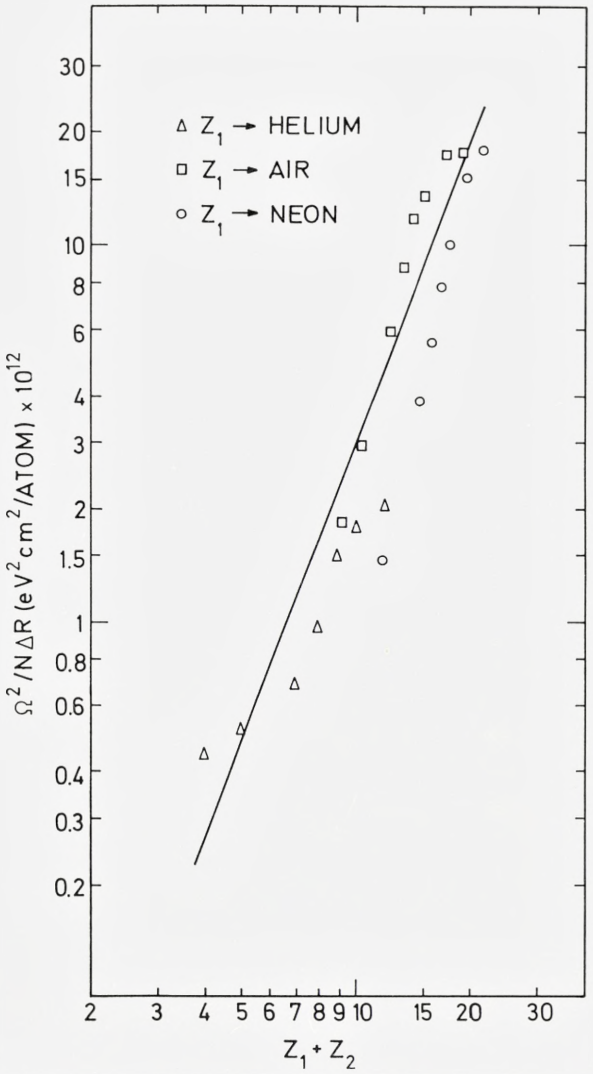

Figure 9. Relative straggling $\Omega^2/N\Delta R$ at constant velocity ($0.9\ v_0$) as a function of $(Z_1 + Z_2)$. Also shown is the theoretical curve (eq. (7)).

in the stopping power in aligned single crystals, and no clear indication of Z_1 oscillations of the same kind have been found in the straggling in a random material.

The present measurements show that the functional dependence of straggling on Z_1, Z_2, and energy, is rather well accounted for by Eq. (7). Further,

the absolute values of straggling agree with the theory within a factor of two. It means that Eq. (7) is well suited for first-order estimates of the straggling in the forward-directed beam.

Some evidence of Z_2 oscillations in stopping power have been found, but further experimental investigations are needed. At present, it is not clear whether these oscillations are of the same nature as the Z_1 oscillations or whether to some extent they depend also on other mechanisms, such as target density.

Acknowledgements

I am grateful to my colleagues for many stimulating discussions, and to the technical staff at the heavy-ion accelerator for their great help. Special thanks are due to B. Fastrup for suggesting this experiment and for his continued interest in the work, and to E. Horsdal Pedersen for his assistance in the data-taking. I am also indebted to J. U. Andersen, J. A. Davies, and J. Lindhard for constructive comments, and to Alice Grandjean for her help in preparing the manuscript.

Institute of Physics, University of Aarhus
8000 Aarhus C, Denmark

References

1. W. White and R. M. Mueller, Phys. Rev. **187** (1969) 499.
2. A. van Wijngaarden and H. E. Duckworth, Can. J. Phys. **40** (1962) 1749.
3. J. R. MacDonald, J. H. Ormrod, and H. E. Duckworth, Z. Naturforsch. **21a** (1966) 130.
4. J. H. Ormrod and H. E. Duckworth, Can. J. Phys. **41** (1963) 1424.
5. J. H. Ormrod, J. R. MacDonald, and H. E. Duckworth, Can. J. Phys. **43** (1965) 275.
6. J. H. Ormrod, Can. J. Phys. **46** (1968) 497.
7. B. Fastrup, P. Hvelplund, and C. A. Sautter, Mat. Fys. Medd. Dan. Vid. Selsk. **35** (1966) 10.
8. P. Hvelplund and B. Fastrup, Phys. Rev. **165** (1968) 408.
9. B. Fastrup, A. Borup, and P. Hvelplund, Can. J. Phys. **46** (1968) 489.
10. L. Eriksson, J. A. Davies, and P. Jespersgård, Phys. Rev. **161** (1967) 219.
11. F. H. Eisen, Can. J. Phys. **46** (1968) 561.
12. J. Bøttiger and F. Bason, Radiation Effects **2** (1969) 105.
13. F. Bernhard, U. Müller-Jahreis, G. Rockstroh, and S. Schwabe, phys. stat. sol. **35** (1969) 285.
14. N. Bohr, Mat. Fys. Medd. Dan. Vid. Selsk. **18** (1948) 8.
15. J. Lindhard and M. Scharff, Phys. Rev. **124** (1961) 128.
16. J. Lindhard, Vibeke Nielsen, and M. Scharff, Mat. Fys. Medd. Dan. Vid. Selsk. **36** (1968) 10.
17. O. B. Firsov, Soviet Phys. JETP **9** (1959) 1076.
18. Ya. A. Teplova, V. S. Nikolaev, I. S. Dmitriev, and L. N. Fateeva, Soviet Phys. JETP **15** (1962) 31.
19. G. Sidenius, J. Sci. Instr. **1** (1968) 657.
20. P. K. Weyl, Phys. Rev. **91** (1953) 289.
21. S. K. Allison and C. S. Littlejohn, Phys. Rev. 104 (1956) 959.
22. W. K. Chu, P. D. Bourland, K. H. Wang, and D. Powers, Phys. Rev. **175** (1968) 343.
23. J. Lindhard, M. Scharff, and H. E. Schiøtt, Mat. Fys. Medd. Dan. Vid. Selsk. **33** (1963) 14.

Indleveret til Selskabet den 15. september 1970.
Færdig fra trykkeriet den 17. februar 1971.